Surendra B. Devarakonda
Department of Mechanical,
Materials Engineering,
College of Engineering and Applied Science,
University of Cincinnati,
Cincinnati, OH 45221

Matthew R. Myers
Division of Applied Mechanics,
Center for Devices and
Radiological Health,
U.S. Food and Drug Administration,
Silver Spring, MD 20993

Rupak K. Banerjee[1]
Fellow ASME
Department of Mechanical,
Materials Engineering,
College of Engineering and
Applied Science,
University of Cincinnati,
593 Rhodes Hall, ML 0072,
Cincinnati, OH 45221
e-mail: Rupak.Banerjee@uc.edu

Comparison of Heat Transfer Enhancement Between Magnetic and Gold Nanoparticles During HIFU Sonication

Long procedure times and collateral damage remain challenges in high-intensity focused ultrasound (HIFU) medical procedures. Magnetic nanoparticles (mNPs) and gold nanoparticles (gNPs) have the potential to reduce the acoustic intensity and/or exposure time required in these procedures. In this research, we investigated relative advantages of using gNPs and mNPs during HIFU thermal-ablation procedures. Tissue-mimicking phantoms containing embedded thermocouples (TCs) and physiologically acceptable concentrations (0.0625% and 0.125%) of gNPs were sonicated at acoustic powers of 5.2 W, 9.2 W, and 14.5 W, for 30 s. It was observed that when the concentration of gNPs was doubled from 0.0625% to 0.125%, the temperature rise increased by 80% for a power of 5.2 W. For a fixed concentration (0.0625%), the energy absorption was 1.7 times greater for mNPs than gNPs for a power of 5.2 W. Also, for the power of 14.5 W, the sonication time required to generate a lesion volume of 50 mm^3 decreased by 1.4 times using mNPs, compared with gNPs, at a concentration of 0.0625%. We conclude that mNPs are more likely than gNPs to produce a thermal enhancement in HIFU ablation procedures.
[DOI: 10.1115/1.4040120]

Introduction

High intensity focused ultrasound (HIFU) is a noninvasive method for treating solid tumors and metastatic disease. HIFU has been applied to treat a variety of solid malignant tumors in pancreas, liver, prostate, breast, uterine fibroids, and soft-tissue sarcomas in clinical settings [1–8]. However, several issues have been reported with the use of HIFU for the thermal ablation of deep-seated tumors. Unintended damage during HIFU procedures, such as skin burns and damage to overlying tissues, has been reported [9–12].

One strategy for reducing the adverse effects associated with high intensities and long exposure times in HIFU ablation procedures is to introduce microcapsules and nanoparticles (NPs) at the tumor site [13,14]. Sun et al. [15,16] reported the effects of PLGA-coated Fe_3O_4 microcapsules in HIFU therapy and have found enhancement in hyperthermia due to the microcapsules. However, the microcapsules used in the study are relatively large (500–850 nm). Use of such large size particles may be difficult to translate to clinical studies. In addition, the acoustic powers used for ablation in these studies are relatively high (180–250 W). Similarly, You et al. [17] performed HIFU sonications on bovine liver (ex vivo) and VX2 hepatic carcinoma in rabbits (in vivo). They reported coagulative volumes up to 400 mm^3 using Fe_3O_4-PFH/PLGA nanocapsules, compared with 20 mm^3 for no nanocapsules. However, the effect of different concentrations of the nanocapsules on the HIFU ablation is not reported. Further, the acoustic powers used in this study are very high (120–180 W). Such powers can cause skin burns and damage to neighboring healthy cells [10].

In a previous study, we [14] measured the HIFU-induced temperature rise using embedded thermocouples (TCs) in tissue phantoms with physiological concentrations (0%, 0.0047%, and 0.047%) of magnetic nanoparticles (mNPs). The temperature rise is determined from measurements made away from the TCs, combined with a mathematical inverse algorithm [18] to infer the heat source producing the remote temperature field. We reported that the power required to obtain a lesion volume of 13 mm^3 can be halved with the use of 0.047% mNP concentration, relative to no added particles. Our initial pilot study [19] measured the HIFU induced temperature rise using embedded TCs in tissue phantoms with concentrations (0%, 1%, and 3%) of mNPs; however, concentrations used are very high and nonphysiological.

In a related study, we [20] conducted HIFU sonications in tissue phantoms embedded with 0%, 0.0625%, and 0.125% gold nanoparticles (gNPs). Using MR thermometry, we reported that for a power of 20 W, the lesion volume doubled for a concentration of 0.0625% gNP's and tripled for a 0.125% concentration, when compared to the case of no gNPs. The temperatures obtained from the MR thermometry are known to be an average of all the temperatures within a pixel.

For comparison with the TC-based temperature rises for the mNPs, the MR thermometry measurements involving gNPs are not ideal, owing to the fact that the temperatures obtained from MR thermometry are an average of all temperatures within a pixel. In the present study, we therefore performed additional measurements with gNPs using the same procedure used to measure thermal effects of mNPs. Tissue phantoms with 0.0625% and 0.125% gNPs concentrations by volume were fabricated. Each tissue phantom was embedded with four TCs, and sonications were performed using acoustic powers of 5.2 W, 9.2 W, and 14.5 W. The temperature profiles during the heating and cooling periods were recorded at each embedded TC. An inverse algorithm [18] was used to calculate the beam location and the focal temperature rise. Lesion volumes were determined from the transient temperature values. A comparison was then made with the temperature rise and lesion-volume results from our previous studies [14], conducted using different concentrations (0.0047% and 0.047%) of mNPs. The temperature data for the 0.0625% mNPs concentration were obtained by extrapolation.

Methods

Below is an outline of the protocol for the experimental procedure. Further details of the procedure may be found in previous publications [14,20].

[1]Corresponding author.

Manuscript received December 10, 2017; final manuscript received April 22, 2018; published online May 24, 2018. Assoc. Editor: Spencer P. Lake.

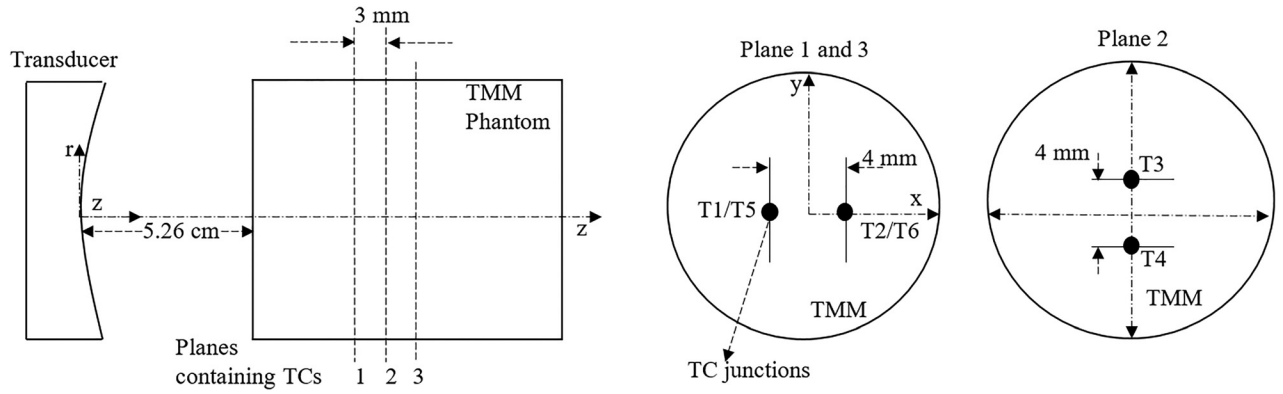

Fig. 1 Schematic of the transducer and TMM phantom embedded with 6 (T1-T6) TCs. The inner diameter of the phantom is 2.5 cm.

Fabrication of Tissue Phantoms. Two cylindrical fixtures with a length of 3 cm and inner diameter of 2.5 cm (volume $\sim 15\,cm^3$) were fabricated. Each fixture is embedded with an array of six thin-wire (Chromega-Constantine) TCs (labeled T1-T6) with the diameter of 0.003 in, arranged in three layers (Fig. 1). A 15-mL gelrite-based tissue-mimicking material (TMM) was prepared according to the protocol of King et al. [21]. In addition to the TMM components, 0.0625% and 0.125% gNPs were incorporated into the mixture. The gNP concentrations differ from the mNP concentrations because the gNP concentrations are chosen to match those of a previous study involving MR thermography [20].

Sonication Procedure. The source of the ultrasound is an H102 transducer (Sonic Concepts Inc., Bothell, WA), which has a focal length of 6.26 cm, outer diameter of 6.4 cm, and inner diameter of 2.2 cm. The transducer operating frequency is 1.025 MHz. For sonication, the beam focus was positioned in the plane of T1–T2 (Fig. 1), in such a way that T1 and T2 recorded approximately the same temperature rise for a sonication period of 10 s. The temperature rise on the full functional array, i.e., thermocouples, T1, T2, T3, T4, and T6 (Fig. 1), was recorded for the 30 s heating period, as well as 20 s of cooling. Thermocouple T5 suffered a malfunction and was not able to record temperature data. Three acoustic power levels were considered—5.2 W, 9.2 W, and 14.5 W. Sonication at each location was performed 3 times ($n = 3$). The temperature of the phantom prior to sonication was 24 °C.

Micro-Computed Tomography Imaging. During pouring of the TMM into the fixture, TC wires could be displaced slightly from their original position. Therefore, to determine the precise location of the TCs, high-resolution micro-CT (Inveon Multimodality System, Siemens Inc., Munich, Germany) was used to scan the tissue phantoms. The adjusted locations of the TC junctions obtained from the micro-CT were used in the inverse algorithm [18].

Beam Localization Within Thermocouple Array. To determine the focal temperature, the beam location within the TC array was ascertained using an inverse algorithm [18]. In the inverse algorithm, the coordinates of the beam focus, relative to the TC coordinates just obtained from the CT scans, are treated as unknowns. The location of the beam is adjusted until the difference between the computed temperature rise at the array nodes and experimentally measured values at those locations is minimized. The beam focus is located by the coordinates yielding the minimum error.

Focal Temperature. Once the beam location was determined using the localization procedure, it was used in a solution to the heat equation in the form of an exponential integral [18,22], to determine the temperature at locations and times of interest. In the exponential-integral solution, the temperature as a function of time at a distance r from the beam axis is given by:

$$T(r,t) = \frac{\alpha I_0 r_0^2}{2\kappa\rho_0 c_p}\left[Ei\left(\frac{-r^2}{r_0^2}\right) - Ei\left(\frac{-r^2}{r_0^2\left(1+\frac{4\kappa t}{r_0^2}\right)}\right)\right] \tag{1a}$$

where $Ei(x)$ is the exponential integral

$$Ei(x) = -\int_{-x}^{\infty}\frac{e^{-s}}{s}ds \tag{1b}$$

Here, r is the radial coordinate, r_0 is the beam radius of the Gaussian intensity distribution, α is the absorption coefficient, which is a function of NP concentration. I_0 is the intensity on the beam axis, κ is the thermal diffusivity, ρ_0 is the density, and c_p is the specific heat of TMM. The properties of the TMM are presented in Table 1.

To calculate the focal temperature at the concentration of 0.0625% mNPs, for which temperature data are not available, a linear extrapolation of the intensity and beam radius were performed for the mNP concentrations (0%, 0.0047%, and 0.047%) presented in our previous study [14]. The extrapolated intensity and beam radius are then used in Eq. (1) to calculate the focal temperatures at the concentration of 0.0625% mNPs. Additionally, to determine the total uncertainty in the temperature estimates in this study, a 6% uncertainty was added to the standard deviation of temperature for the three trials. The 6% value was determined in a previous study by the authors [18] to be the uncertainty in temperature estimates performed using the exponential-integral technique in the focal plane. Further information can be found in our previous study [14].

Thermal Dose. The thermal dose corresponding to a temperature $T(t)$ was calculated using the method developed by Sapareto and Dewey [23]. The thermal dose parameter is given by

$$t_{43}(x,y,z) = \int_{t=0}^{t=t_{\text{final}}} R^{43-T(t)}dt \tag{2}$$

Table 1 Properties of the TMM

Property	Value
Density, ρ_0	1040 kg/m^3
Absorption coefficient, α	45 dB/m
Specific heat, C_p	4064 J/kg K
Thermal diffusivity, κ	1.4×10^{-7} m^2/s

where t_{43} is the thermal dose at the reference temperature of 43 °C, t_{final} is the treatment (sonication + cooling) time, $T(t)$ is the temperature (in °C) as a function of time obtained experimentally at the focal location, and

$$R = \begin{cases} 0.5 & \text{if } T(t) \geq 43\,^{\circ}\text{C} \\ 0.25 & \text{otherwise} \end{cases} \quad (3)$$

For all thermal-dose calculations, a trapezoidal scheme has been used to perform the integration with a time increment of $\Delta t = 0.5$ s.

Lesion Volume. A lesion is defined as a volume of cells exposed to a thermal dose [24] equal to or greater than a threshold value believed to lead to cell necrosis. An initial guess of z-plane was made for assessing the radial variation of temperature and the lesion boundary at the z-plane. First, the radial temperature profile in the z-plane was obtained from Eqs. (1*a*) and (1*b*). Subsequently, the temperature was then used in Eq. (2) to determine the thermal dose in the z-plane. If the thermal dose was not within 3% of 240 equivalent minutes, the guess for z-plane was updated and the procedure repeated. The radial extent of the 240 min point was found using a similar iterative process using Eqs. (1*a*), (1*b*), and (2). The lesion volume calculation proceeded by considering each lesion section of axial length (dz) to be a truncated cone of height dz, and base radii $r_{i,240}$ and $r_{i+1,240}$ for the ith section. The total volume (V) is calculated by summing up the volumes of the truncated cones

$$V = \sum \frac{1}{3}\pi\left(r_{i,240}^2 + r_{i,240}r_{i+1,240} + r_{i+1,240}^2\right)dz \quad (4)$$

Further details of the lesion volume calculation can be found in our previous study [14].

Results

Below, comparisons are performed between the present gNP data and the data previously acquired for different mNP concentrations (0.0047% and 0.047%). The results for the different mNP concentrations are reported in Devarakonda et al. [14]. The measured temperatures are averaged over the three trials for each acoustic power level. Results are presented as mean ± SD.

Figure 2 shows the HIFU-induced focal temperature variations with time for three mNPs (0.0047%, 0.047% and 0.0625%*; where * denotes extrapolated data) and two gNP concentrations (0.0625% and 0.125%) for three power levels (5.2 W, 9.2 W, and 14.5 W). The focal temperatures were derived using Eq. (1), as described above and in our previous studies [14]. The temperature trace for the 0.047% mNP concentration is similar to that for the 0.0625% gNP concentration at all powers. The temperature rise for the 0.0625% mNP is higher than that for the equivalent concentration of gNP's, and at the higher powers is within 10% of the temperature rise for the 0.125% gNP concentration. As the power increases, the temperature traces become more clustered, i.e., the temperature rise is less sensitive to NP type or concentration. This is especially true for the concentrations greater than 0.0047%.

The amount of absorbed ultrasound energy for the 0.0625% mNPs and 0.125% gNPs, derived from the initial slope of the temperature trace [13], is provided in Table 2. An initial time of 2.5 s is chosen to compute the slopes. The 2.5 s time is chosen because it is long enough that the temperature rise due to ultrasound attenuation elevated above the TC noise level on the remote TCs, yet short enough that appreciable diffusion has not occurred yet [19]. The absorbed energy values in the table are normalized by the absorbed energy for the 0.0625% gNP case. As with the temperatures in Fig. 2, the absorbed energies grow closer together (ratios of initial slopes approach) as the power increases. The temperatures at the end-of-sonication time ($t = 30$ s) are plotted in

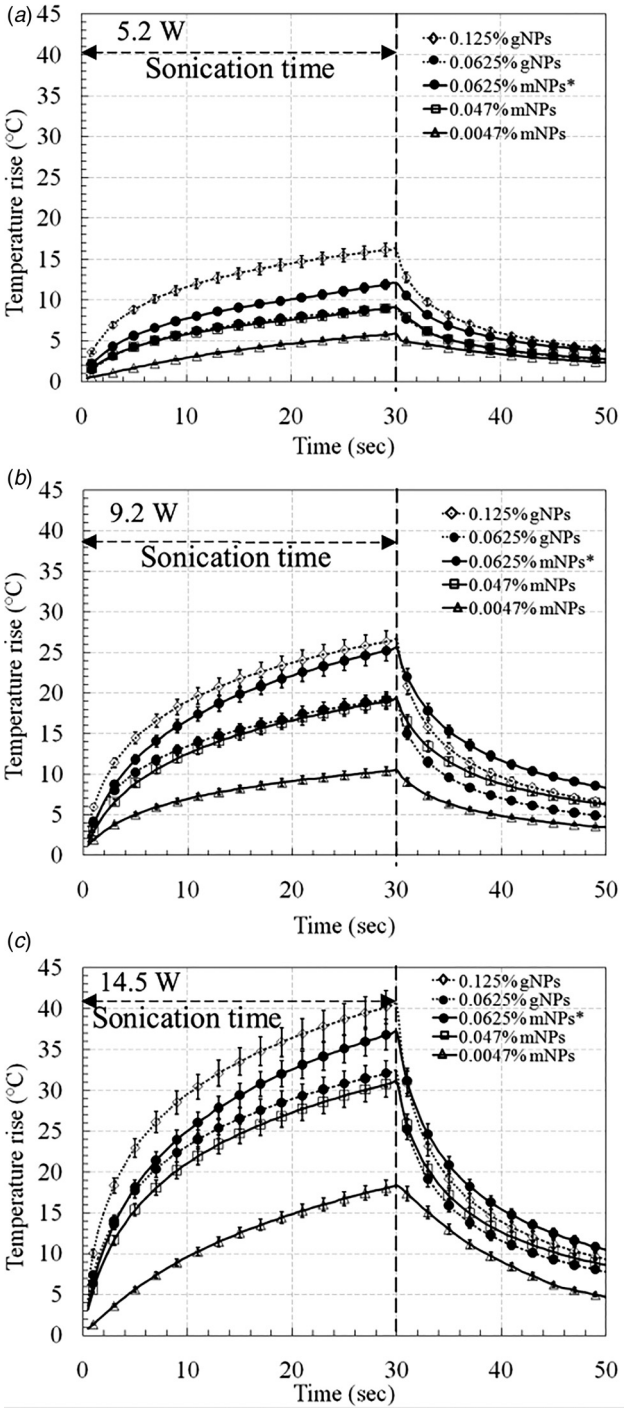

Fig. 2 Comparison of temperature rise (°C) with time (sec) for gNPs (0.0625% and 0125% concentrations) and mNPs (0.0047%, 0.047%, and 0.0625%* concentrations) for (*a*) 5.2, (*b*) 9.2, and (*c*) 14.5 W acoustic powers. The temperature rise values for 0.0625% mNPs concentration have been obtained by extrapolation (*). The sonication and the cooling periods are 30 s and 20 s, respectively.

Table 2 The ratio of the initial slope of the temperature trace for 0.0625%* mNPs and 0.125% gNPs, normalized by the slope for the case of 0.0625% gNPs at each selected power (5.2, 9.2, and 14.5 W).

	5.2 W	9.2 W	14.5 W
0.0625% mNPs	1.7	1.2	1.1
0.125% gNPs	2	1.4	1.3

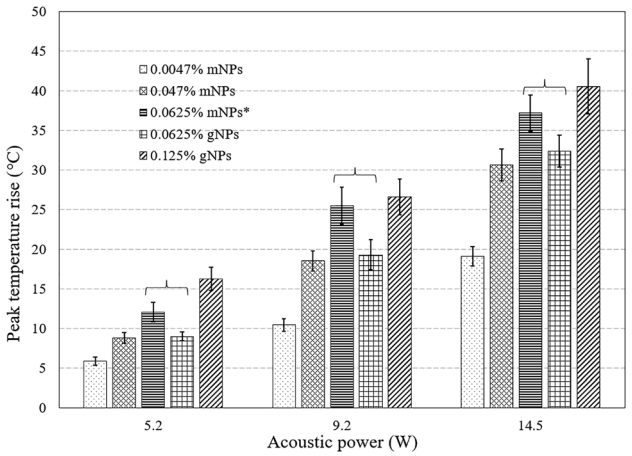

Fig. 3 Comparison of peak focal temperature rise (°C) of gNPs (0.0625% and 0125% concentrations) and mNPs (0.0047%, 0.047%, and 0.0625%* concentrations) for 5.2, 9.2, and 14.5 W acoustic powers. The peak temperature rise values for 0.0625% mNPs concentration have been obtained by extrapolation (*). Measurements for each time point have been conducted in triplicate ($n = 3$). ⌐¬represents comparison of peak temperature rise (° C) for same (0.0625%) concentration of mNPs and gNPs.

Fig. 3 for the powers of 5.2, 9.2, and 14.5 W for gNPs and mNPs. At a fixed concentration (0.0625%), the peak temperatures for mNPs are higher than gNPs by 34% ($= (12-9) \times 100/9$), 31% ($= (25.5-19.3) \times 100/19.3$), and 15% ($= (37.2-32.4) \times 100/32.4$) for the powers of 5.2, 9.2, and 14.5 W, respectively. Based upon a two-sided t-test, the differences between the two 0.0625% concentrations are significant ($p = 0.05$) at all power levels.

Figure 4 provides the sonication time required to produce a 50 mm^3 lesion (14 mm in axial extent and 1.3 mm maximum radius). At all NP concentrations, the decrease in procedure time relative to the zero-NP baseline is substantial—at least an order of magnitude decrease in time is achieved for all concentrations and powers, except for the 0.0047% mNP concentration at 14.7 W. At the highest power, 0.0625% concentrations of mNPs and gNPs produced the given lesion within 38±8 s and 54±13 s, respectively (Fig. 5). The statistical difference is moderate and the p value is 0.14, which can be improved with larger sample size.

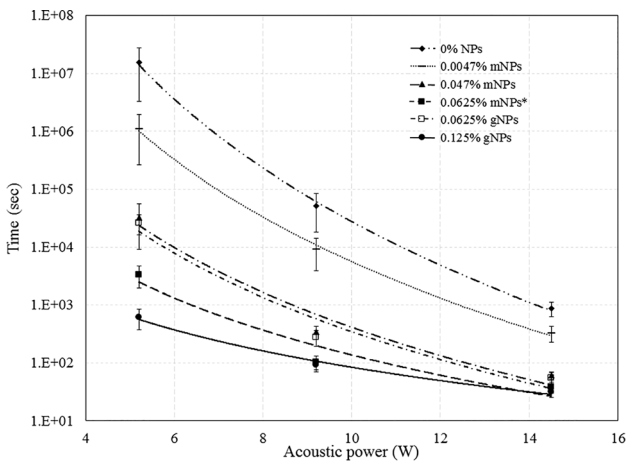

Fig. 4 Sonication time required to achieve a lesion volume of 50 mm^3 (1.3 mm in radial direction and 14 mm in axial direction) for mNPs (concentrations of 0.0047%, 0.047%, and 0.0625%*), gNPs (0.0625% and 0.125%), and no NPs (0%) for 5.2, 9.2, and 14.5 W acoustic powers. The values for 0.0625% mNPs concentration have been calculated using the extrapolated temperature data (*). Calculations for each point have been conducted in triplicate ($n = 3$). *Y*-axis is in logarithmic scale.

Discussion

By placing the TCs remote from the ultrasound beam, potentially large TC artifacts [25] have been avoided. Likewise, the errors associated with positioning a narrow beam atop a TC have been avoided using the array of TCs and the optimization method. The price paid for the advantages of the present temperature measurement technique employing remote TCs is the need for precise knowledge of the TC locations. This information is acquired with CT imaging.

The improvement in sonication time, relative to the baseline 0% NPs, reduced as the power increased (Fig. 4), for both types of NPs. For example, at a power of 5.2 W, a reduction in sonication time of 4 orders of magnitude relative to the control case is observed. At the 14.5 W power, the reduction in sonication time is about a factor of 30. This reduction in thermal enhancement may be due in part to the fact that at higher powers, cell death occurs as a result of intense local absorption of ultrasound energy, rather than diffusion of heat from hotter locations. Thus, even in the absence of NPs, lesion formation becomes faster. Additionally, some of the heat generated by the NPs raises the cell temperature beyond the point of necrosis, at which point, the energy is no longer contributing to lesion formation. Thus, at higher powers, the thermal enhancement decreases, in terms of sonication time required to achieve a certain lesion volume. Still, the 30 fold reduction in sonication time at the 14.5 W power level would likely be welcome in a clinical setting.

The comparison between the mNPs and gNPs can be roughly summarized with the statement that the 0.047% mNP concentration behaved very similarly to the 0.0625%. Whether this makes the mNP's preferable clinically depends in part on the biocompatibility and MR compatibility of the two types of NPs.

Proposed Analysis. In our previous work [26], we have reported that the HIFU absorption in media embedded with NPs depends on the thermal processes (*viscous*, *phonon layers,* and *intrinsic absorption*) at the interface of metal NPs and on the *physical* properties (such as density) of the media embedded with NPs [27–30]. The theoretical equation for temperature rise (ΔT) due to HIFU attenuation is given as

$$\Delta T = \int_0^t \frac{T_0 \beta v_{nf} \alpha_{nf} P_0}{\rho_{nf} C_{nf} A v_m} e^{\alpha_{nf} v_{nf} t} dt \tag{5}$$

where C_{nf} is the heat capacity, β is thermal expansion coefficient, ρ_{nf} is the density of medium with NPs, v_{nf} is the sound velocity in the medium, α_{nf} is the total attenuation, A is the area of HIFU beam, T_0 is heat wave parameter, v_m is the particle velocity, and P_0 is the HIFU acoustic power. Further details can be obtained from our previous study [26].

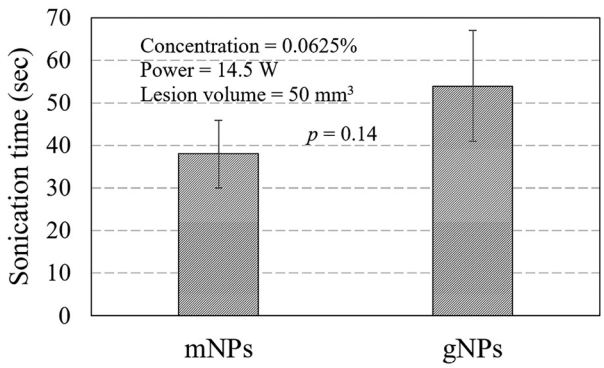

Fig. 5 Sonication time needed to obtain a lesion volume of 50 mm^3 for a concentration of 0.0625% at 14.5 W acoustic power for mNPs and gNPs

At a constant power P_0, the temperature rise is a function of several parameters including T_0, C_{nf}, β, ν_{nf}, ρ_{nf}, and α_{nf} as reported in Eq. (5). The ultrasound velocity is 60% higher in the mNPs than the gNPs [27,31,32], which may be contributing to the increase in temperature rise due to mNPs when compared to gNPs. The density of gNPs being nearly 4 times greater than the mNPs [26] may cause the temperature rise due to gNPs to be lower than the mNPs. Similarly, other parameters such as T_0, β, α_{nf}, and C_{nf} may be contributing to the higher temperature rise in the mNPs in comparison to gNPs.

The temperature rise due to presence of NPs is because of three complex mechanisms (*viscous*, *phonon layers,* and *intrinsic absorption*) occurring at the interfaces of metal NPs. We have previously reported that the effect of temperature rise due to phonon layer is more than the viscous drag effect for mNPs [26]. It is expected that the temperature rise due to viscous drag is the dominating phenomenon than the phonon layer for gNPs. However, further investigation is needed to analyze the mechanism behind the temperature rise due to mNPs and gNPs.

Funding Data

- Division of Chemical, Bioengineering, Environmental, and Transport Systems, National Science Foundation (Grant No. CBET-1403356).

References

[1] Bailey, M. R., Couret, L. N., Sapozhnikov, O. A., Khokhlova, V. A., ter Haar, G., Vaezy, S., Shi, X., Martin, R., and Crum, L. A., 2001, "Use of Overpressure to Assess the Role of Bubbles in Focused Ultrasound Lesion Shape In Vitro," Ultrasound Med. Biol., **27**(5), pp. 695–708.

[2] Mesiwala, A. H., Farrell, L., Wenzel, H. J., Silbergeld, D. L., Crum, L. A., Winn, H. R., and Mourad, P. D., 2002, "High-Intensity Focused Ultrasound Selectively Disrupts the Blood-Brain Barrier In Vivo," Ultrasound Med. Biol., **28**(3), pp. 389–400.

[3] Kyriakou, Z., Corral-Baques, M. I., Amat, A., and Coussios, C. C., 2011, "HIFU-Induced Cavitation and Heating in Ex Vivo Porcine Subcutaneous Fat," Ultrasound Med. Biol., **37**(4), pp. 568–579.

[4] McLaughlan, J., Rivens, I., Leighton, T., and Ter Haar, G., 2010, "A Study of Bubble Activity Generated in Ex Vivo Tissue by High Intensity Focused Ultrasound," Ultrasound Med. Biol., **36**(8), pp. 1327–1344.

[5] Oh, K. S., Han, H., Yoon, B. D., Lee, M., Kim, H., Seo, D. W., Seo, J. H., Kim, K., Kwon, I. C., and Yuk, S. H., 2014, "Effect of HIFU Treatment on Tumor Targeting Efficacy of Docetaxel-Loaded Pluronic Nanoparticles," Colloids Surf. B, **119**, pp. 137–144.

[6] Miller, A. D., 2013, "Lipid-Based Nanoparticles in Cancer Diagnosis and Therapy," J. Drug Deliv., **2013**, p. 165981.

[7] O'Neill, B. E., Vo, H., Angstadt, M., Li, K. P., Quinn, T., and Frenkel, V., 2009, "Pulsed High Intensity Focused Ultrasound Mediated Nanoparticle Delivery: Mechanisms and Efficacy in Murine Muscle," Ultrasound Med. Biol., **35**(3), pp. 416–424.

[8] Lai, P., McLaughlan, J. R., Draudt, A. B., Murray, T. W., Cleveland, R. O., and Roy, R. A., 2011, "Real-Time Monitoring of High-Intensity Focused Ultrasound Lesion Formation Using Acousto-Optic Sensing," Ultrasound Med. Biol., **37**(2), pp. 239–252.

[9] Furusawa, H., Namba, K., Thomsen, S., Akiyama, F., Bendet, A., Tanaka, C., Yasuda, Y., and Nakahara, H., 2006, "Magnetic Resonance-Guided Focused Ultrasound Surgery of Breast Cancer: Reliability and Effectiveness," J. Am. Coll. Surg., **203**(1), pp. 54–63.

[10] Li, J.-J., Xu, G.-L., Gu, M.-F., Luo, G.-Y., Rong, Z., Wu, P.-H., and Xia, J.-C., 2007, "Complications of High Intensity Focused Ultrasound in Patients With Recurrent and Metastatic Abdominal Tumors," World J. Gastroenterol.: WJG, **13**(19), pp. 2747–2751.

[11] Day, E. S., Morton, J. G., and West, J. L., 2009, "Nanoparticles for Thermal Cancer Therapy," ASME J. Biomech. Eng., **131**(7), p. 074001.

[12] Devarakonda, S., Ahmad Reza Dibaji, S., Hariharan, P., Myers, M. R., and Banerjee, R. K., 2016, "Characterization of Focal Location During High-Intensity Focused Ultrasound Ablation in a Tissue Phantom Using Remote Thermocouple Arrays," ASME J. Med. Dev., **10**(2), p. 020949.

[13] Ahmad Reza Dibaji, S., Al-Rjoub, M. F., Myers, M. R., and Banerjee, R. K., 2014, "Enhanced Heat Transfer and Thermal Dose Using Magnetic Nanoparticles During HIFU Thermal Ablation—An In-Vitro Study," ASME J. Nanotechnol. Eng. Med., **4**(4), p. 040902.

[14] Devarakonda, S. B., Myers, M. R., Giridhar, D., Dibaji, S. A., and Banerjee, R. K., 2017, "Enhanced Thermal Effect Using Magnetic Nano-Particles During High-Intensity Focused Ultrasound," PloS One, **12**(4), p. e0175093.

[15] Sun, Y., Zheng, Y., Li, P., Wang, D., Niu, C., Gong, Y., Huang, R., Wang, Z., and Ran, H., 2014, "Evaluation of Superparamagnetic Iron Oxide-Polymer Composite Microcapsules for Magnetic Resonance-Guided High-Intensity Focused Ultrasound Cancer Surgery," BMC Cancer, **14**(1), p. 800.

[16] Sun, Y., Zheng, Y., Ran, H., Zhou, Y., Shen, H., Chen, Y., Chen, H., Krupka, T. M., Li, A., Li, P., and Wang, Z., 2012, "Superparamagnetic PLGA-Iron Oxide Microcapsules for Dual-Modality U.S./MR Imaging and High Intensity Focused U.S. Breast Cancer Ablation," Biomaterials, **33**(24), pp. 5854–5864.

[17] You, Y., Wang, Z., Ran, H., Zheng, Y., Wang, D., Xu, J., Wang, Z., Chen, Y., and Li, P., 2016, "Nanoparticle-Enhanced Synergistic HIFU Ablation and Transarterial Chemoembolization for Efficient Cancer Therapy," Nanoscale, **8**(7), pp. 4324–4339.

[18] Hariharan, P., Dibaji, S. A., Banerjee, R. K., Nagaraja, S., and Myers, M. R., 2014, "Localization of Focused-Ultrasound Beams in a Tissue Phantom, Using Remote Thermocouple Arrays," IEEE Trans. Ultrason. Ferroelectr. Freq. Control, **61**(12), pp. 2019–2031.

[19] Gadsden, E., Aguilar, M. T., Smoller, B. R., and Jewell, M. L., 2011, "Evaluation of a Novel High-Intensity Focused Ultrasound Device for Ablating Subcutaneous Adipose Tissue for Noninvasive Body Contouring: Safety Studies in Human Volunteers," Aesthet. Surg. J., **31**(4), pp. 401–410.

[20] Devarakonda, S. B., Myers, M. R., Lanier, M., Dumoulin, C., and Banerjee, R. K., 2017, "Assessment of Gold Nanoparticle-Mediated-Enhanced Hyperthermia Using MR-Guided High-Intensity Focused Ultrasound Ablation Procedure," Nano Lett., **17**(4), pp. 2532–2538.

[21] King, R. L., Liu, Y., Maruvada, S., Herman, B. A., Wear, K. A., and Harris, G. R., 2011, "Development and Characterization of a Tissue-Mimicking Material for High-Intensity Focused Ultrasound," IEEE Trans. Ultrason. Ferroelectr. Freq. Control, **58**(7), pp. 1397–1405.

[22] Dillon, C. R., Vyas, U., Payne, A., Christensen, D. A., and Roemer, R. B., 2012, "An Analytical Solution for Improved HIFU SAR Estimation," Phys. Med. Biol., **57**(14), pp. 4527–4544.

[23] Sapareto, S. A., and Dewey, W. C., 1984, "Thermal Dose Determination in Cancer Therapy," Int. J. Radiat. Oncol. Biol., Phys., **10**(6), pp. 787–800.

[24] Righetti, R., Kallel, F., Stafford, R. J., Price, R. E., Krouskop, T. A., Hazle, J. D., and Ophir, J., 1999, "Elastographic Characterization of HIFU-Induced Lesions in Canine Livers," Ultrasound Med. Biol., **25**(7), pp. 1099–1113.

[25] Morris, H., Rivens, I., Shaw, A., and Haar, G. T., 2008, "Investigation of the Viscous Heating Artefact Arising From the Use of Thermocouples in a Focused Ultrasound Field," Phys. Med. Biol., **53**(17), pp. 4759–4776.

[26] Bera, C., Devarakonda, S. B., Kumar, V., Ganguli, A. K., and Banerjee, R. K., 2017, "The Mechanism of Nanoparticle-Mediated Enhanced Energy Transfer During High-Intensity Focused Ultrasound Sonication," Phys. Chem. Chem. Phys., **19**, pp. 19075–19082.

[27] Allegra, J. R., and Hawley, S. A., 1972, "Attenuation of Sound in Suspensions and Emulsions: Theory and Experiments," J. Acoust. Soc. Am., **51**(5B), pp. 1545–1564.

[28] Simons, S., 1964, "On the Interaction of Long Wavelength Phonons With Thermal Phonons," Proc. Phys. Soc., **83**(5), p. 749.

[29] Brawer, S., 1973, "Contribution to Sound Absorption in Disordered Solids at Low Temperatures," Phys. Rev. B, **7**(4), pp. 1712–1717.

[30] Pinkerton, J. M. M., 1949, "The Absorption of Ultrasonic Waves in Liquids and Its Relation to Molecular Constitution," Proc. Phys. Soc. Sect. B, **62**(2), p. 129.

[31] Se-yuen, M., Yee-kong, N., and Kam-wah, W., 2000, "Measurement of the Speed of Sound in a Metal Rod," Phys. Educ., **35**(6), p. 439.

[32] Jiří, E., 2015, "Measurement of Elastic Modulus and Ultrasonic Wave Velocity by Piezoelectric Resonator," Eur. J. Phys., **36**(1), p. 015017.